

Nonlinear Decay of Quantum Confined Magnons in Itinerant Ferromagnets

Kh. Zakeri^{1,*}, A. Hjelt¹, I. V. Maznichenko,² P. Buczek², and A. Ernst^{3,4}

¹*Heisenberg Spin-Dynamics Group, Physikalisches Institut, Karlsruhe Institute of Technology, Wolfgang-Gaede-Strasse 1, D-76131 Karlsruhe, Germany*

²*Department of Engineering and Computer Sciences, Hamburg University of Applied Sciences, Berliner Tor 7, D-20099 Hamburg, Germany*

³*Institute for Theoretical Physics, Johannes Kepler University, Altenberger Strasse 69, A-4040 Linz, Austria*

⁴*Max-Planck-Institut für Mikrostrukturphysik, Weinberg 2, D-06120 Halle, Germany*



(Received 29 January 2021; accepted 6 April 2021; published 28 April 2021)

Quantum confinement leads to the emergence of several magnon modes in ultrathin layered magnetic structures. We probe the lifetime of these quantum confined modes in a model system composed of three atomic layers of Co grown on different surfaces. We demonstrate that the quantum confined magnons exhibit nonlinear decay rates, which strongly depend on the mode number, in sharp contrast to what is assumed in the classical dynamics. Combining the experimental results with those of linear-response density-functional calculations we provide a quantitative explanation for this nonlinear damping effect. The results provide new insights into the decay mechanism of spin excitations in ultrathin films and multilayers and pave the way for tuning the dynamical properties of such structures.

DOI: [10.1103/PhysRevLett.126.177203](https://doi.org/10.1103/PhysRevLett.126.177203)

Understanding the processes behind the excitation and relaxation of spin excitations in low-dimensional magnetic structures is one of the most intriguing research directions in solid-state physics. A detailed knowledge of the fundamental mechanisms involved in such processes is the key to understanding many different phenomena. Examples are ultrafast magnetization reversal by magnetic field pulses [1] or by torque transfer from spin-polarized currents [2–4], vortex core gyration driven magnon emission [5], sub-picosecond demagnetization by photon pulses [6–9], and spin dependence of image potential states at ferromagnetic surfaces [10]. In addition to its fundamental impact, a complete understanding of magnetic relaxation mechanisms is of great importance for designing efficient spin-based devices as the power consumption of such devices is determined by the damping [11–13].

The excited state of a magnetic system is described by magnons, the quanta of spin waves. The relaxation of such an excited state can, in principle, involve the dissipation of magnetic energy in several ways. In approaches based on the classical dynamics, damping is described by a phenomenological damping parameter, commonly referred to as Gilbert damping [14–16]. This description is only valid in the case of uniform ferromagnetic resonance, i.e., the magnons with zero wave vector ($q = 0$), under some circumstances [17–21]. For magnons with $q \neq 0$, the relaxation of a certain magnon mode can involve its dissipation to other magnons (multimagnon scattering process) or, in the case of itinerant magnets, their dissipation into single-particle electron-hole pair excitations, known as Stoner excitations. In both cases, one expects an

increase of the magnon decay rate with the magnon energy, since usually the density of both magnon as well as Stoner states increases with energy.

In structurally well-defined low-dimensional magnetic structures one expects additional magnon modes due to the effects associated with quantum confinement. In ultrathin magnetic films composed of N atomic layers one expects the existence of $n = 0, 1, \dots, N - 1$ magnon modes, as a result of quantum confinement in the direction perpendicular to the structure [22–28]. Each magnon mode is characterized by its eigenvalue and eigenstate and hence differ from the others. These magnon modes spread in the energy-momentum space [29–31]. The dispersion relation of all confined magnon modes has recently been probed [32–34]. However, the relaxation mechanism of these magnon modes remains hitherto unexplored.

In this Letter, we report on the decay rate of the quantum confined magnon modes in a model system. We show that the quantum confined magnons exhibit decay rates, which are nonlinear in energy and strongly depend on the magnons' mode number n . This observation is in contrast to what is commonly discussed in the framework of the classical dynamics. Combining the results of linear-response time-dependent density-functional theory calculations with adiabatic spin dynamics calculations, we provide a quantitative explanation for the damping of quantum confined magnons.

Experiments are performed by means of spin-polarized high-resolution electron energy-loss spectroscopy (SPEELS) on ultrathin Co films with a thickness of three atomic layers epitaxially grown on Ir(001), Ir(111), and

Cu(001). In SPEELS a monochromatic spin-polarized beam is scattered from the sample surface and the scattered electrons are analyzed in terms of their energy and wave vector transfer. Figure 1(a) shows typical SPEELS spectra recorded on a 3 monolayer (ML) Co film on Ir(001). The spectra are recorded for the two possible incoming spin states. I_{\downarrow} (I_{\uparrow}) represents the intensity spectrum when the spin polarization of the incoming beam is parallel (antiparallel) to the sample magnetization [26]. The difference spectrum, shown in the lower panel, contains all the possible spin-flip excitations of down to up, including magnons [26,35]. The data are recorded at $(q_x, q_y) = (0.3, 0.3) \text{ \AA}^{-1}$, corresponding to the in-plane wave vector $q_{\parallel} = 0.42 \text{ \AA}^{-1}$ along the $\Gamma\text{-}\bar{M}$ direction. In order to unambiguously determine the magnon excitation energy and the lifetime, the difference spectra recorded at different wave vectors are fitted with three lines, corresponding to the expected three magnon modes of the system. Each line includes a Lorentzian line shape, convoluted with the experimental broadening [36,37]. An example is shown in Fig. 1(b), where the experimental difference spectrum ($I_{\downarrow} - I_{\uparrow}$) is shown together with the fits. The magnon dispersion relation was measured by probing the magnons at different wave vectors and along different symmetry directions of the surface Brillouin zone and the results are summarized in Fig. 1(c). For a quantitative description, the magnon properties were calculated based on first principles. It has been shown that a quantitative description of the experimental magnon bands can only be provided when spin-dependent many-body correlation effects on the majority Co spins are taken into consideration [32,38]. In Fig. 1(c) the magnonic band structure calculated using this approach is presented as the color map. The band structure is presented by plotting

the magnon Bloch spectral function. Since the adiabatic approach does not account for the decay of magnons, the spectral function exhibits sharp peak at the places where magnon modes exist. The approach accounts, however, for all the details of the structure (e.g., the reconstruction of the Ir surface) and provides an unambiguous way for the determination of magnon properties, e.g., their real space localization and density of magnon states [34].

To understand the decay mechanism of magnons, we calculated the frequency ω and wave vector \mathbf{q} -dependent transverse dynamical spin susceptibility $\chi(\omega, \mathbf{q})$, using linear-response time-dependent density-functional theory (LRTDDFT) [39–42]. In the first step, the so-called Kohn-Sham susceptibility was calculated, based on first principles, and in the second step, $\chi(\omega, \mathbf{q})$ was calculated self-consistently (see [41] for details). In Fig. 1(d) we provide an example of $\text{Im}\chi(\omega, \mathbf{q})$ at $(q_x, q_y) = (0.3, 0.3)$. Since in this approach both magnons and Stoner excitations are adequately taken into account, $\text{Im}\chi(\omega, \mathbf{q})$ can directly be compared to the difference spectrum shown in Fig. 1(b) [43–49]. In order to have a better comparison, we convolute the results with the experimental resolution. Similar to the experiment, one observes all the three confined magnon modes. Each mode exhibits its own decay rate.

In order to quantify the decay rates of different quantum confined magnon modes, we carefully analyze the intrinsic broadening of the modes and the results are summarized in Fig. 2(a), indicating that different quantum confined magnon modes show different decay rates. Moreover, to address the effects associated with the film morphology and the hybridization of the electronic structures of the film with those of the underlying substrate, similar experiments were performed on 3 ML Co films grown on Cu(001) and Ir(111) [26,50–52]. The results are presented along with

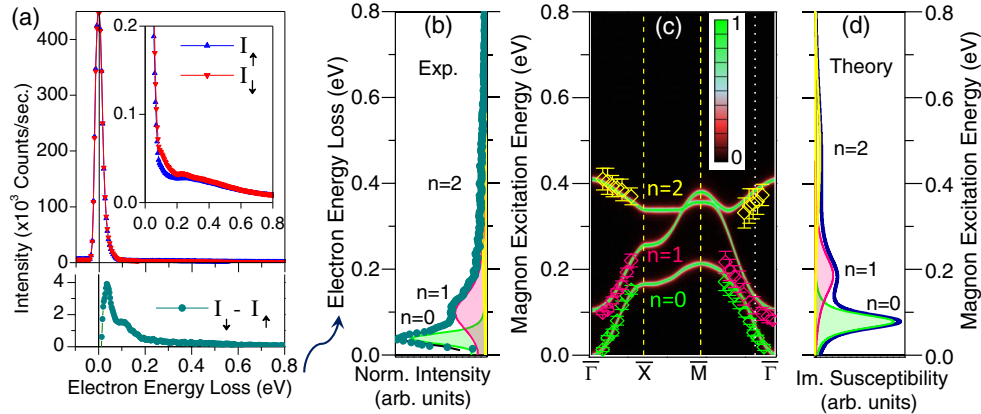


FIG. 1. (a) SPEELS spectra recorded on 3 ML Co/Ir(001) at $(q_x, q_y) = (0.3, 0.3) \text{ \AA}^{-1}$. I_{\downarrow} (I_{\uparrow}) represents the spectrum when the spin polarization of the incoming electron beam is parallel (antiparallel) to the magnetization. The difference spectrum $I_{\downarrow} - I_{\uparrow}$ is shown in the lower panel. (b) The difference spectrum and the fits used to extract the dispersion relation and the lifetime of different quantum confined magnons indicated by $n = 0\text{--}2$. (c) The dispersion relation of all confined magnon modes. The experimental data are shown by symbols and the calculated magnon Bloch spectral function using our adiabatic approach is presented as the color map. The dotted line shows the place in the surface Brillouin zone, where the spectra shown in (a) and (b) are recorded. (d) $\text{Im}\chi(\omega, \mathbf{q})$ at $(q_x, q_y) = (0.3, 0.3) \text{ \AA}^{-1}$ calculated by LRTDDFT and convoluted with the experimental broadening.

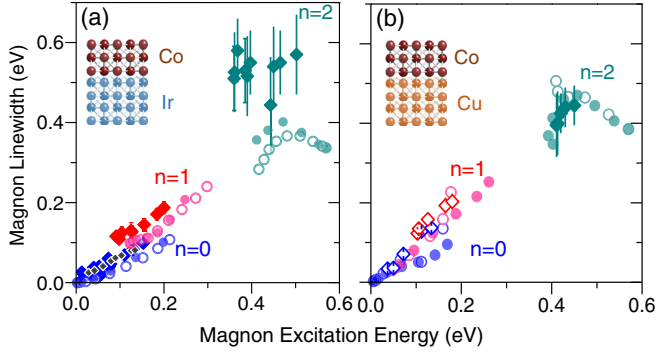


FIG. 2. The magnon linewidth versus energy for all quantum confined magnon modes in 3 ML Co on (a) Ir(001) and (b) Cu(001). The experimental results are shown by diamonds and the results of LRTDDFT calculations are shown by circles. The filled (open) symbols represent the data along the $\bar{\Gamma}$ - \bar{M} ($\bar{\Gamma}$ - \bar{X}) direction. The black diamonds in (a) represent the results of the $n = 0$ magnon mode of 3 ML Co/Ir(111).

those of the Co(001)/Ir(001) system. We note that, due to the geometrical consideration, e.g., different lattice constants, these systems possess different magnonic band structures. The main aim here is to understand the decay rate of these magnon modes, with respect to the mode number and mode energy and quantify the different contributions to the damping. In a similar manner we also analyze the line broadening of all the magnon modes as calculated by LRTDDFT and the results are summarized in Fig. 2, indicating a very good agreement with the experimental results. A careful analysis of the experimental and theoretical results indicates that (i) each magnon mode possesses its own decay rate, (ii) for all studied systems the magnon mode with $n = 0$ exhibits the lowest damping, and (iii) the magnon linewidth versus energy is nonlinear, which becomes more pronounced for the higher order modes.

Generally, the main source of damping in itinerant ferromagnets, such as the systems studied here, is the result of the decay of these collective modes into single-particle Stoner excitations, a mechanism known as Landau damping. In the case of ultrathin magnetic films on substrates, the hybridizations of the electronic states of the film with those of the substrate can open additional decay channels and lead to stronger damping of the magnons. Hence the Landau damping in layered ferromagnets on nonmagnetic substrates can be very complex, compared to that of the single-element bulk ferromagnets [41,42,53,54]. LRTDDFT calculations start with the *ab initio* calculations of electronic structures using experimental geometrical structures as inputs. The electronic structures are then used to calculate $\chi(\omega, \mathbf{q})$. Since the approach treats both magnons and Stoner excitations on the same basis, the Landau damping is fully taken into account.

Looking at the results shown in Fig. 2, the linewidth of each magnon mode increases with energy in a nonlinear

fashion. The increase of the magnon linewidth with energy is because the decay probability of a magnon into a Stoner pair increases with energy. This probability depends on the details of the involved electronic bands and hence is not a simple linear function with energy. This scenario is even more complex when considering the fact that the electronic states of the film hybridize very strongly with those of the substrate. The so-called Landau hot spots, where the decay of magnons to Stoner excitations takes place, become increasingly important for higher energy magnons [41,42,53]. As it is apparent from Fig. 2, both the experimental and theoretical results indicate that these magnon modes exhibit different (nonlinear) decay rates. Hence the origin of the mode-dependent decay rate lies in the Landau damping. The effect can be understood based on the fact that for the $n \neq 0$ magnon modes the perpendicular magnon wave vector is nonzero ($q_{\perp} \neq 0$). Hence the Stoner pairs with nonzero perpendicular momentum enter the picture. The possibility of the decay into such Stoner modes shortens the lifetime of magnons with $n \neq 0$. In the LRTDDFT calculations, both the magnons and Stoner excitations are put on an equal footing and hence this effect is clearly observed in the calculated linewidth.

The second possible decay channel is the decay of a certain magnon mode to the other possible magnon (or phonon) modes that share the same energy. As an example, in Fig. 3(a), the processes of magnon decay of the $n = 1$ magnon mode at the $\bar{\Gamma}$ point is shown by the solid arrows. In addition, small variations in the film thickness can lead to additional magnon modes, which may also share the same energy with this mode [55]. In order to mimic this effect in Fig. 3(a), we also show the magnonic bands of a film with the same geometrical structure but with a thickness of 4 ML. The results are shown by the light-gray color in Fig. 3(a). Since the $n = 1$ mode can also degenerate with the modes of such a system, one needs to consider such decay rates. The decay rates of this kind are shown by the dashed arrows in Fig. 3(a). In the LRTDDFT calculations, such effects are not taken into account. In order to generalize the decay process of a certain magnon mode to all the other possible quasiparticles, the damping may be written as [53,56]

$$\Gamma(\mathbf{q}, \omega) = \sum_{n,m} \int_{\Omega_{BZ}} \mathcal{P}_{\mathbf{k}}^n \mathcal{P}_{\mathbf{k}-\mathbf{q}}^m \delta(E - E_{\mathbf{k}}^n - E_{\mathbf{k}-\mathbf{q}}^m) d\mathbf{k}, \quad (1)$$

where $\mathcal{P}_{\mathbf{k}}^n$ and $\mathcal{P}_{\mathbf{k}-\mathbf{q}}^m$ denote the probability of finding a magnon, phonon, or electron with the wave vector \mathbf{k} in the n th and $\mathbf{k} - \mathbf{q}$ in the m th band, and $E_{\mathbf{k}}^n$ ($E_{\mathbf{k}-\mathbf{q}}^m$) describes the energy dispersion of the n th (m th) quasiparticle band. The term shall account for all the possible decay channels through which a magnon with the energy $\hbar\omega$ and wave vector \mathbf{q} can decay into single-particle Stoner pairs, other magnons, and phonons, satisfying the energy conservation rule $E_{\mathbf{q}} = \hbar\omega = E_{\mathbf{k}} - E_{\mathbf{k}-\mathbf{q}}$. Note that, in the case of

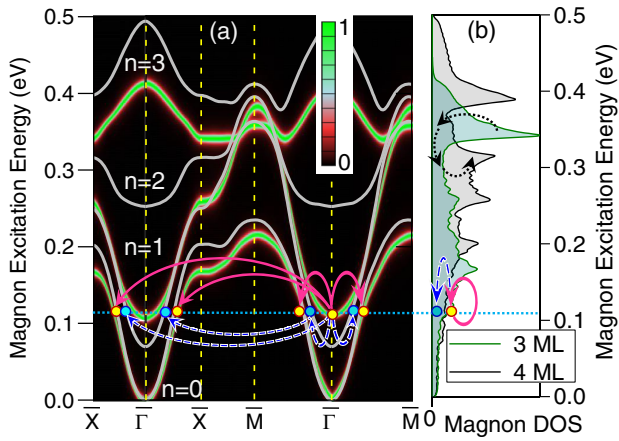


FIG. 3. (a) The magnon Bloch spectral function of 3 ML Co on Ir(001) based on adiabatic calculations. The color scale represents the amplitude of the spectral function. The magnonic bands of a 4 ML film are also shown by the light-gray curves. The multi-magnon scattering processes of the $n = 1$ magnon mode within the 3 ML terraces are shown by the solid arrows. The decay processes within the terraces of different thicknesses (3 and 4 ML) are shown by the dashed arrows. (b) The magnonic density of states for a 3 and 4 ML film calculated based on the adiabatic approach. The direct decay of the $n = 1$ magnon mode of the 3 ML film to the $n = 0$ and $n = 1$ of a 4 ML film is illustrated with the dashed arrows. The horizontal dotted light-blue line denotes the energy of the bottom of the $n = 1$ mode of the 3 ML system (at $q_{\parallel} = 0$), where this mode can scatter to the other modes. The indirect decay of the $n = 2$ magnon mode of the 3 ML film to the $n = 2$ and $n = 1$ modes of the 4 ML film is schematically shown by the dotted black arrows.

electronic bands, the transition should also account for the conservation of magnon's total angular momentum, meaning that only the transitions between the bands with opposite spins should be considered. In order to describe the decay of magnons into bosonic quasiparticles, e.g., phonons and other possible magnon states, according to Eq. (1), one should be able to analyze the different possibilities of such decays in the energy-momentum space. In metallic ferromagnets, the phonon energies are rather low (< 20 meV) and the magnon-phonon coupling is rather weak. Hence, the magnon decay by phonons becomes of minor importance for high-energy magnons. The main decay channel of the magnon-boson kind is the one associated with their decay into other magnon modes. In order to estimate the strength of such decay rates, we calculated the magnonic density of states (DOS). The results of such calculations are presented in Fig. 3(b). We also present the magnon DOS of a film composed of four atomic layers. The probability of finding magnons in a given state (indicated by circles) can therefore be simply estimated by analyzing the magnon DOS. The magnon-magnon decay is directly proportional to the number of initial and final magnon states, which may contribute to such a process ($\mathcal{P}_{\mathbf{k}}^n$ and $\mathcal{P}_{\mathbf{k}-\mathbf{q}}^m$). If such states are largely

available, the magnon decay can occur with a large probability. Looking at the data presented in Fig. 3, one realizes that such decay process can occur with a large probability, since there are enough initial and final magnon states that can contribute to these kinds of magnon decays (solid arrows in Fig. 3). In addition to the intrinsic magnon-magnon decay, the variation in the film thickness can also lead to a magnon decay. For example, if the film is composed of terraces with the thickness of 3 and 4 ML, the $n = 1$ magnon mode of the 3 ML terraces can decay into the $n = 1$ and $n = 0$ magnon modes of the terraces with the thickness of 4 ML. Such a process can happen with a large probability, as shown by the dashed arrows in Fig. 3. Interestingly the $n = 2$ mode of the 3 ML region can, in principle, decay to the other modes of the 4 ML region via an inelastic process in which the magnons are decayed in a two-step process [dotted arrows in Fig. 3(b)]. The process can occur with a high probability because near the states of the $n = 2$ mode of the 3 ML region there exist a large number of states caused by the $n = 2$ and $n = 1$ modes of the 4 ML region. Co films on Cu(001) grow in a layer-by-layer fashion. Because of the reconstruction of the Ir(001) surface, the roughness of Co films on this surface is larger than that of the Co films on Cu(001). This leads to a larger magnon decay of this kind and explains the larger experimental linewidth of this mode as compared to the Co/Cu(001) system and also to the results of LRTDDFT.

In summary, aiming for a fundamental understanding of the decay processes of quantum confined magnons in layered ferromagnets, we investigated the lifetime of these excitations in a model system composed of 3 ML Co grown on different surfaces over a wide range of energy and momentum. It was observed that the quantum confined magnons exhibit nonlinear decay rates. The decay rates strongly depend on the mode number. In the phenomenological approach of classical dynamics, the decay rate is assumed to be linear. Such an assumption is not valid for the quantum confined magnons. Combining the experimental results with those of LRTDDFT calculations, we provide a quantitative explanation for this nonlinear damping. In addition, since the quantum confinement leads to the emergence of several magnon branches, the decay processes as a result of magnon-magnon scattering become also important. These multimagnon decay processes become stronger due to variations in the film thickness. Our results indicate that the main source of damping in layered structures made of itinerant ferromagnets is due to the Landau damping as a result of their decay into Stoner excitations. Hence in order to design layered ferromagnets with low damping, first the electronic structure should be tuned such that the Landau damping is suppressed. Moreover, atomically flat films are required to achieve a low damping. In addition to the fact that our results provide new insights into the decay mechanism of spin excitations

in ultrathin films and multilayers, they provide guidelines regarding how the dynamical properties of layered structures can be tuned.

Kh.Z. acknowledges funding from the Deutsche Forschungsgemeinschaft (DFG) through the Heisenberg Programme ZA 902/3-1 and ZA 902/6-1 and the DFG Grant No. ZA 902/4-1. Kh.Z. thanks the Physikalisches Institut for hosting the group and providing the necessary infrastructure.

*khalil.zakeri@partner.kit.edu

- [1] I. Tudosa, C. Stamm, A. B. Kashuba, F. King, H. C. Siegmann, J. Stöhr, G. Ju, B. Lu, and D. Weller, The ultimate speed of magnetic switching in granular recording media, *Nature (London)* **428**, 831 (2004).
- [2] J. C. Slonczewski, Current-driven excitation of magnetic multilayers, *J. Magn. Magn. Mater.* **159**, L1 (1996).
- [3] J. A. Katine, F. J. Albert, R. A. Buhrman, E. B. Myers, and D. C. Ralph, Current-Driven Magnetization Reversal and Spin-Wave Excitations in Co/Cu/Co Pillars, *Phys. Rev. Lett.* **84**, 3149 (2000).
- [4] K. Garello, C. O. Avci, I. M. Miron, M. Baumgartner, A. Ghosh, S. Auffret, O. Boulle, G. Gaudin, and P. Gambardella, Ultrafast magnetization switching by spin-orbit torques, *Appl. Phys. Lett.* **105**, 212402 (2014).
- [5] S. Wintz, V. Tiberkevich, M. Weigand, J. Raabe, J. Lindner, A. Erbe, A. Slavin, and J. Fassbender, Magnetic vortex cores as tunable spin-wave emitters, *Nat. Nanotechnol.* **11**, 948 (2016).
- [6] E. Beaurepaire, J.-C. Merle, A. Daunois, and J.-Y. Bigot, Ultrafast Spin Dynamics in Ferromagnetic Nickel, *Phys. Rev. Lett.* **76**, 4250 (1996).
- [7] C. D. Stanciu, F. Hansteen, A. V. Kimel, A. Kirilyuk, A. Tsukamoto, A. Itoh, and Th. Rasing, All-Optical Magnetic Recording with Circularly Polarized Light, *Phys. Rev. Lett.* **99**, 047601 (2007).
- [8] B. Koopmans, G. Malinowski, F. D. Longa, D. Steiauf, M. Fähnle, T. Roth, M. Cinchetti, and M. Aeschlimann, Explaining the paradoxical diversity of ultrafast laser-induced demagnetization, *Nat. Mater.* **9**, 259 (2010).
- [9] C.-H. Lambert, S. Mangin, B. S. D. C. S. Varaprasad, Y. K. Takahashi, M. Hehn, M. Cinchetti, G. Malinowski, K. Hono, Y. Fainman, M. Aeschlimann, and E. E. Fullerton, All-optical control of ferromagnetic thin films and nanostructures, *Science* **345**, 1337 (2014).
- [10] A. B. Schmidt, M. Pickel, M. Donath, P. Buczek, A. Ernst, V. P. Zhukov, P. M. Echenique, L. M. Sandratskii, E. V. Chulkov, and M. Weinelt, Ultrafast Magnon Generation in an Fe Film on Cu(100), *Phys. Rev. Lett.* **105**, 197401 (2010).
- [11] K. Zakeri, Elementary spin excitations in ultrathin itinerant magnets, *Phys. Rep.* **545**, 47 (2014).
- [12] J. Walowski and M. Münzenberg, Perspective: Ultrafast magnetism and THz spintronics, *J. Appl. Phys.* **120**, 140901 (2016).
- [13] K. Zakeri, Terahertz magnonics: Feasibility of using terahertz magnons for information processing, *Physica (Amsterdam)* **549C**, 164 (2018).
- [14] M. Sparks, Ferromagnetic resonance in thin films. II. Theory of linewidths, *Phys. Rev. B* **1**, 3856 (1970).
- [15] T. L. Gilbert, Classics in magnetics a phenomenological theory of damping in ferromagnetic materials, *IEEE Trans. Magn.* **40**, 3443 (2004).
- [16] R. D. McMichael and P. Krivosik, Classical model of extrinsic ferromagnetic resonance linewidth in ultrathin films, *IEEE Trans. Magn.* **40**, 2 (2004).
- [17] R. D. McMichael, D. J. Twisselmann, and A. Kunz, Localized Ferromagnetic Resonance in Inhomogeneous Thin Films, *Phys. Rev. Lett.* **90**, 227601 (2003).
- [18] J. Lindner, K. Lenz, E. Kosubek, K. Baberschke, D. Spoddig, R. Meckenstock, J. Pelzl, Z. Frait, and D. L. Mills, Non-gilbert-type damping of the magnetic relaxation in ultrathin ferromagnets: Importance of magnon-magnon scattering, *Phys. Rev. B* **68**, 060102(R) (2003).
- [19] B. Heinrich, Spin relaxation in magnetic metallic layers and multilayers, in *Ultrathin Magnetic Structures III* (Springer-Verlag, Berlin, 2005), pp. 143–210.
- [20] G. Woltersdorf and B. Heinrich, Two-magnon scattering in a self-assembled nanoscale network of misfit dislocations, *Phys. Rev. B* **69**, 184417 (2004).
- [21] K. Zakeri, J. Lindner, I. Barsukov, R. Meckenstock, M. Farle, U. von Hörsten, H. Wende, W. Keune, J. Rucker, S. S. Kalarickal, K. Lenz, W. Kuch, K. Baberschke, and Z. Frait, Spin dynamics in ferromagnets: Gilbert damping and two-magnon scattering, *Phys. Rev. B* **76**, 104416 (2007).
- [22] T. Balashov, A. F. Takács, W. Wulfhekel, and J. Kirschner, Magnon Excitation with Spin-Polarized Scanning Tunneling Microscopy, *Phys. Rev. Lett.* **97**, 187201 (2006).
- [23] C. L. Gao, A. Ernst, G. Fischer, W. Hergert, P. Bruno, W. Wulfhekel, and J. Kirschner, Spin Wave Dispersion on the Nanometer Scale, *Phys. Rev. Lett.* **101**, 167201 (2008).
- [24] J. Rajeswari, H. Ibach, and C. M. Schneider, Standing Spin Waves in Ultrathin Magnetic Films: A Method to Test for Layer-Dependent Exchange Coupling, *Phys. Rev. Lett.* **112**, 127202 (2014).
- [25] H. Ibach, High resolution electron energy loss spectroscopy of spin waves in ultra-thin film: The return of the adiabatic approximation?, *Surf. Sci.* **630**, 301 (2014).
- [26] Kh. Zakeri and J. Kirschner, *Probing Magnons by Spin-Polarized Electrons* (Springer, Berlin, Heidelberg, 2013), Chap. 7, pp. 84–99.
- [27] T. Balashov, P. Buczek, L. Sandratskii, A. Ernst, and W. Wulfhekel, Magnon dispersion in thin magnetic films, *J. Phys. Condens. Matter* **26**, 394007 (2014).
- [28] P. Buczek, S. Thomas, A. Marmodoro, N. Buczek, X. Zubizarreta, M. Hoffmann, T. Balashov, W. Wulfhekel, K. Zakeri, and A. Ernst, Spin waves in disordered materials, *J. Phys. Condens. Matter* **30**, 423001 (2018).
- [29] A. Taroni, A. Bergman, L. Bergqvist, J. Hellsvik, and O. Eriksson, Suppression of Standing Spin Waves in Low-Dimensional Ferromagnets, *Phys. Rev. Lett.* **107**, 037202 (2011).
- [30] L. Bergqvist, A. Taroni, A. Bergman, C. Etz, and O. Eriksson, Atomistic spin dynamics of low-dimensional magnets, *Phys. Rev. B* **87**, 144401 (2013).
- [31] O. Eriksson, A. Bergman, L. Bergqvist, and J. Hellsvik, *Atomistic Spin Dynamics: Foundations and Applications* (Oxford University Press, New York, 2016).

- [32] Y. J. Chen, K. Zakeri, A. Ernst, H. J. Qin, Y. Meng, and J. Kirschner, Group Velocity Engineering of Confined Ultrafast Magnons, *Phys. Rev. Lett.* **119**, 267201 (2017).
- [33] K. Zakeri, Magnonic crystals: Towards terahertz frequencies, *J. Phys. Condens. Matter* **32**, 363001 (2020).
- [34] K. Zakeri, H. Qin, and A. Ernst, Unconventional magnonic surface and interface states in layered ferromagnets, *Commun. Phys.* **4**, 18 (2021).
- [35] J. Prokop, W. X. Tang, Y. Zhang, I. Tudosa, T. R. F. Peixoto, K. Zakeri, and J. Kirschner, Magnons in a Ferromagnetic Monolayer, *Phys. Rev. Lett.* **102**, 177206 (2009).
- [36] Y. Zhang, T. H. Chuang, K. Zakeri, and J. Kirschner, Relaxation Time of Terahertz Magnons Excited at Ferromagnetic Surfaces, *Phys. Rev. Lett.* **109**, 087203 (2012).
- [37] K. Zakeri, Y. Zhang, T. H. Chuang, and J. Kirschner, Magnon Lifetimes on the Fe(110) Surface: The Role of Spin-Orbit Coupling, *Phys. Rev. Lett.* **108**, 197205 (2012).
- [38] H. J. Qin, S. Tsurkan, A. Ernst, and K. Zakeri, Experimental Realization of Atomic-Scale Magnonic Crystals, *Phys. Rev. Lett.* **123**, 257202 (2019).
- [39] H. A. Mook and D. Tocchetti, Neutron Scattering Measurements of the Generalized Susceptibility $\chi(q, e)$ for Ni, *Phys. Rev. Lett.* **43**, 2029 (1979).
- [40] S. Y. Savrasov, Linear Response Calculations of Spin Fluctuations, *Phys. Rev. Lett.* **81**, 2570 (1998).
- [41] P. Buczek, A. Ernst, and L. M. Sandratskii, Different dimensionality trends in the Landau damping of magnons in iron, cobalt, and nickel: Time-dependent density functional study, *Phys. Rev. B* **84**, 174418 (2011).
- [42] P. Buczek, A. Ernst, and L. M. Sandratskii, Interface Electronic Complexes and Landau Damping of Magnons in Ultrathin Magnets, *Phys. Rev. Lett.* **106**, 157204 (2011).
- [43] J. Callaway, C. S. Wang, and D. G. Laurent, Magnetic susceptibility and spin waves in ferromagnetic metals, *Phys. Rev. B* **24**, 6491 (1981).
- [44] J. Hong and D. L. Mills, Spin excitations in ferromagnetic Ni: Electrons and neutrons as a probe, *Phys. Rev. B* **61**, R858 (2000).
- [45] R. B. Muniz, A. T. Costa, and D. L. Mills, Microscopic theory of spin waves in ultrathin ferromagnetic films: Fe on W(110), *J. Phys. Condens. Matter* **15**, S495 (2003).
- [46] A. T. Costa, R. B. Muniz, and D. L. Mills, Spin waves and their damping in itinerant ultrathin ferromagnets: Intermediate wave vectors, *Phys. Rev. B* **74**, 214403 (2006).
- [47] R. B. Muniz, A. T. Costa, and D. L. Mills, Spin dynamics of itinerant electron ferromagnetic nanostructures, *IEEE Trans. Magn.* **44**, 1974 (2008).
- [48] A. T. Costa, R. B. Muniz, J. X. Cao, R. Q. Wu, and D. L. Mills, Magnetism of an Fe monolayer on W(110), *Phys. Rev. B* **78**, 054439 (2008).
- [49] A. T. Costa, R. B. Muniz, S. Lounis, A. B. Klautau, and D. L. Mills, Spin-orbit coupling and spin waves in ultrathin ferromagnets: The spin-wave Rashba effect, *Phys. Rev. B* **82**, 014428 (2010).
- [50] Y. Meng, K. Zakeri, A. Ernst, T. H. Chuang, H. J. Qin, Y. J. Chen, and J. Kirschner, Direct evidence of antiferromagnetic exchange interaction in Fe(001) films: Strong magnon softening at the high-symmetry (m)over-bar point, *Phys. Rev. B* **90**, 174437 (2014).
- [51] T. H. Chuang, K. Zakeri, A. Ernst, Y. Zhang, H. J. Qin, Y. Meng, Y. J. Chen, and J. Kirschner, Magnetic properties and magnon excitations in Fe(001) films grown on Ir(001), *Phys. Rev. B* **89**, 174404 (2014).
- [52] K. Zakeri, Probing of the interfacial Heisenberg and Dzyaloshinskii–Moriya exchange interaction by magnon spectroscopy, *J. Phys. Condens. Matter* **29**, 013001 (2017).
- [53] H. J. Qin, K. Zakeri, A. Ernst, L. M. Sandratskii, P. Buczek, A. Marmodoro, T. H. Chuang, Y. Zhang, and J. Kirschner, Long-living terahertz magnons in ultrathin metallic ferromagnets, *Nat. Commun.* **6**, 6126 (2015).
- [54] H. J. Qin, K. Zakeri, A. Ernst, and J. Kirschner, Temperature Dependence of Magnetic Excitations: Terahertz Magnons above the Curie Temperature, *Phys. Rev. Lett.* **118**, 127203 (2017).
- [55] E. Michel, H. Ibach, C. M. Schneider, D. L. R. Santos, and A. T. Costa, Lifetime and mean free path of spin waves in ultrathin cobalt films, *Phys. Rev. B* **94**, 014420 (2016).
- [56] P. Park, K. Park, T. Kim, Y. Kousaka, K. H. Lee, T. G. Perring, J. Jeong, U. Stuhr, J. Akimitsu, M. Kenzelmann, and J.-G. Park, Momentum-Dependent Magnon Lifetime in the Metallic Noncollinear Triangular Antiferromagnet CrB₂, *Phys. Rev. Lett.* **125**, 027202 (2020).